Scripta Materialia 170 (2019) 62–66

Contents lists available at ScienceDirect

Scripta Materialia

journal homepage: www.elsevier.com/locate/scriptamat

Grain boundary inter-connections of ∑5 boundaries in a high purity iron with a uniform microstructure

Weiguo Wang [a,d,*], Yunkai Cui [a], Gregory S. Rohrer [b], Changhui Cai [a], Song Chen [a,d], Xinfu Gu [c], Yan Lin [a,d]

[a] School of Materials Science and Engineering, Fujian University of Technology, Fuzhou 350118, China
[b] Department of Materials Science and Engineering, Carnegie Mellon University, Pittsburgh, PA 15213-3890, USA
[c] School of Materials Science and Engineering, University of Science and Technology Beijing, Beijing 100083, China
[d] Fujian Provincial Key Laboratory of Advanced Materials Processing and Application, Fuzhou 350118, China

ARTICLE INFO

Article history:
Received 6 April 2019
Received in revised form 21 May 2019
Accepted 22 May 2019
Available online xxxx

Keywords:
High purity iron
∑5 boundary
Grain boundary inter-connection

ABSTRACT

Electron backscatter diffraction was used to measure the grain boundary character distribution of high purity (99.999%) iron with a uniform microstructure produced by multi-directional forging and recrystallization. Subsets of the grain boundaries were analyzed by the five-parameter method and it was found that grain boundary inter-connections of ∑5 boundaries had a strong preference for {0 1 3}/{0 1 3}. A crystallographic analysis indicates that the {0 1 3}/{0 1 3} grain boundary inter-connection is exactly located on the closest packed plane of the ∑5 coincidence site lattice.

As defined previously [1,2], grain boundary (GB) inter-connection (GBIC) refers to the coupling of two crystallographic planes from the two abutting grains terminating at the GB position. GBIC is usually expressed as $\{h_1\ k_1\ l_1\}/\{h_2\ k_2\ l_2\}$, where $\{h_1\ k_1\ l_1\}$ and $\{h_2\ k_2\ l_2\}$ are the Miller indexes of the two inter-connected crystallographic planes. This formulation is consistent with the concept of GB plane matching previously described by Pumphreys [3], Randle [4] and Palumbo [5]. It may be argued that the $\{h_1\ k_1\ l_1\}/\{h_2\ k_2\ l_2\}$ interconnection has little meaning at the atomic scale because the atoms in the GB region usually relax away from their exact lattice positions. Nevertheless, the GBIC is the most reasonable parameter that can be determined from orientation data and defines the character or structure of a GB. For example, GBIC determines the atomic configurations in a GB region such as the dislocation structure (usually the secondary dislocation structure), the shape and size of free volume, the faceting mode and even the precipitation behavior [6–9]. The typical application of GBIC may be found in the GB engineering (GBE) [10] of low to medium stacking fault energy (SFE) face centered cubic (FCC) metals in which coherent twin boundary or coherent ∑3 boundary with a {1 1 1}/{1 1 1} GBIC is pursued [11,12]. In this case, thermal mechanical processing (TMP) is applied to increase the concentration of the {1 1 1}/{1 1 1} GBIC to 50% or more to improve the inter-granular corrosion resistance and high temperature creep strength [13–16]. However, it is not so easy to introduce the coherent twin boundary (or coherent ∑3 boundary) into body centered cubic (BCC) metals. This is because the twinning plane is {1 1 2}, and this is the third closest packed plane. As an alternate approach to grain boundary engineer BCC metals, it may be possible to tap the potential of some other low ∑ coincidence site lattice (CSL) [17,18] boundaries including ∑5, ∑7 and ∑9. To manipulate the population of low ∑ CSL boundaries and improve the overall properties through GBE, it is first necessary to study the GBICs of these boundaries. As for the ∑3 boundary in FCC metals, the structure and properties of boundaries with the same ∑ value, but different GBICs may be very different [1]. Transmission electron microscopy (TEM) may be used to characterize the GBICs at the atomic level under the so-called edge-on condition [19]. However, it is only possible to conduct this measurement on a very limited number of GBs and, as a result, the observation may not be statistically significance. Hence, the present work uses an integrated method involving electron backscatter diffraction (EBSD), GB segment extraction, the partitioning of GBs based on crystallography, stereology-based five parameter analysis (FPA) [20,21] and crystallographic analysis to study the GBICs in a BCC polycrystal. Because impurities and texture (preferred orientations) could affect GB migration during recrystallization and thus affect the final population of GBICs, a high purity iron with a uniform microstructure is used in present work. Because this is the first investigation of this topic, only the GBICs of ∑5 boundaries are considered.

* Corresponding author at: School of Materials Science and Engineering, Fujian University of Technology, Fuzhou 350118, China.
E-mail address: wang_weiguo@vip.163.com (W. Wang).

https://doi.org/10.1016/j.scriptamat.2019.05.033
1359-6462/

A zone-melted high purity iron bar (99.999%, mass fraction) with the diameter of 10 mm and height of 20 mm was machined into a cuboid sample with a geometry of 15 mm × 7 mm × 7 mm. The sample was subjected to multi-directional forging (MDF) with true strain of 4, followed by a recrystallization annealing at 630 °C for 10 min. Such processing was repeated at least four times so that a uniform microstructure was obtained in the sample. The details of the processing are provided in reference [2]. Then, a smaller sample with a size of 8 mm × 6 mm × 1 mm was cut from the bigger sample using a high precision saw (Beuhler EM 5000). The smaller sample was mechanically polished with emery paper followed by electro-chemical polishing in an ice-cooled solution of perchloric acid:glacial acid = 25:75 (vol%) at 30 V for 4 min. After this two-step polishing, the sample was put into a FEI Nova nano 450 field emission scanning electron microscope (FE-SEM) equipped with an Oxford Aztec facility for EBSD mapping. During the EBSD mapping, the SEM and EBSD systems used an acceleration voltage of 20 kV, a spot size of 4.5, a working distance of 9 mm and a step size 0.5 μm. The field of view of each EBSD map was 500 μm × 400 μm. To ensure the statistical significance of the results, several tens of EBSD maps were recorded from the sample. After EBSD mapping, the band contrast (BC) grain morphology, orientation imaging microscopy (OIM), misorientation distribution (MD) and a section of the orientation distribution function (ODF) were generated through data processing. Because the present work focuses on the GBIC of ∑5 boundaries, it was necessary to extract from the EBSD maps line segments representing the boundaries between two grains. In total, 199,298 GB segments were extracted from 25 EBSD maps. Next, using a process we refer to as "filtering" [2], we identified those GBs with the ∑5 misorientation (⟨1 0 0⟩/36.87°). Using a threshold angular deviation ($\Delta\theta$) of ± 2.5°, only 311 GB segments of ∑5 boundaries were isolated. However, when $\Delta\theta$ was expanded to the value specified by Brandon criterion [22].

$$\Delta\theta = \frac{15^\circ}{\sqrt{\sum}} = \frac{15^\circ}{\sqrt{5}} = 6.7^\circ \tag{1}$$

785 GB segments of ∑5 boundaries were identified. Obviously, the number of GB segments of ∑5 boundaries with angular deviations ranging from ±2.5° to ±6.7° must be 785–311 = 474. The ∑5 boundaries obtained by filtering were then used to compute the grain boundary plane distribution (GBPD) [23] by stereology-based FPA method [2,20,21]. The distribution has units of multiple of a random distribution (MRD). Based on the GBPD results, the GBIC of ∑5 boundaries can be ascertained via the following equation [24].

$$\begin{bmatrix} h_2 \\ k_2 \\ l_2 \end{bmatrix} = R_{[1\,0\,0]/36.87^\circ} \begin{bmatrix} h_1 \\ k_1 \\ l_1 \end{bmatrix} = \begin{bmatrix} 1.0 & 0 & 0 \\ 0 & 0.8 & -0.6 \\ 0 & 0.6 & 0.8 \end{bmatrix} \begin{bmatrix} h_1 \\ k_1 \\ l_1 \end{bmatrix} \tag{2}$$

where $(h_1\ k_1\ l_1)$ is the orientation of one of the maxima in the GBPD, $R_{[1\,0\,0]/36.87^\circ}$ is the misorientation matrix of ∑5 boundaries, and $(h_2\ k_2\ l_2)$ is derived from Eq. (2). When $(h_2\ k_2\ l_2)$ is also one of the maxima in the same GBPD, there is a GBIC of $(h_1\ k_1\ l_1)/(h_2\ k_2\ l_2)$.

Fig. 1 shows the microstructure of the sample as processed. We can see from the BC morphology (Fig. 1a) and OIM (Fig. 1b) that the grain size is uniform and the average grain size is approximately 12 μm. From the ODF section (Fig. 1c), we can see scattered texture components such as {0 0 1}⟨1 0 0⟩, {1 1 2}⟨1 1 0⟩ and {1 1 1}⟨1 1 0⟩. However the texture is very weak with a maximum intensity of only 1.35 which is not very different from that of random (1.0). This is consistent with the OIM image in Fig. 1b. The misorientation distribution (Fig. 1d) is

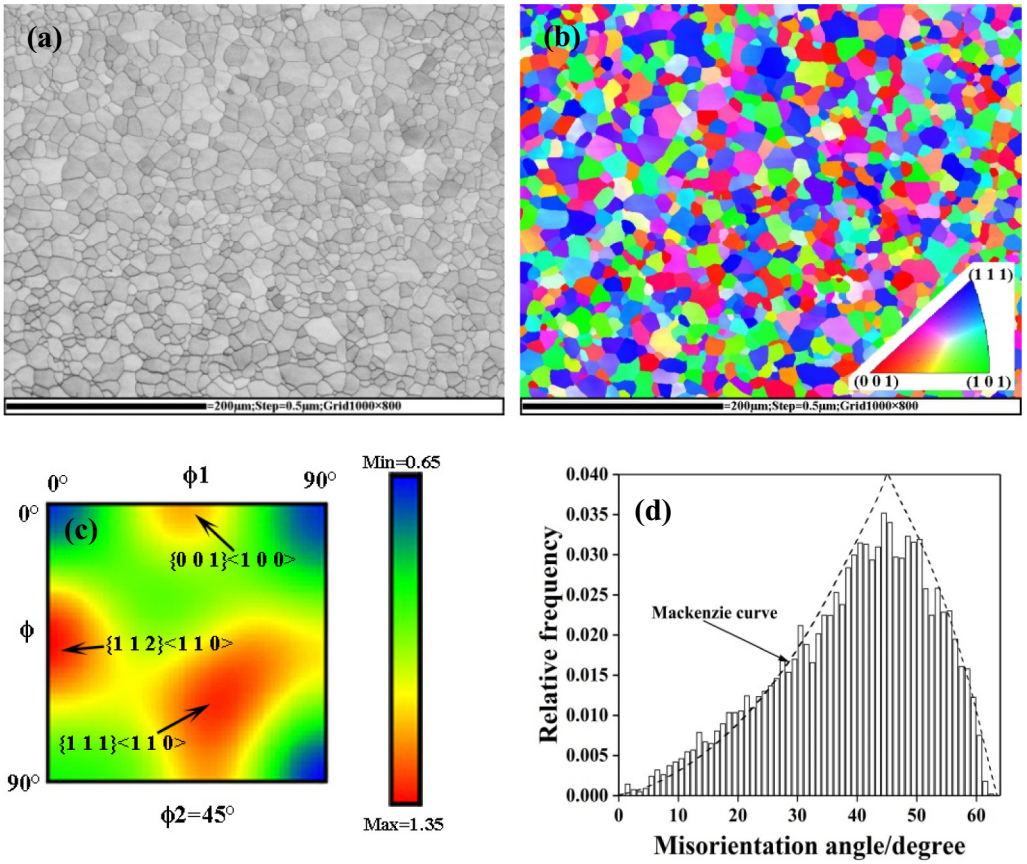

Fig. 1. The microstructure of the sample as processed. (a) band contrast (BC) grain morphology; (b) orientation imaging microscopy (OIM) image; (c)φ2 = 45° section of orientation distribution function (ODF); (d) misorientation distribution.

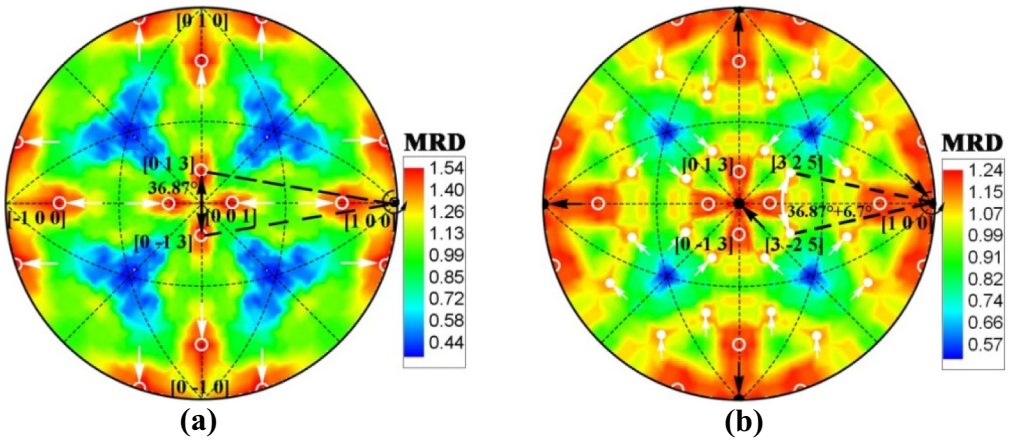

Fig. 2. The GBPDs of ∑5 boundaries as filtered (projected onto (0 0 1)). (a) With angular deviations ±2.5°; (b) with angular deviations ±6.7° (Brandon criterion).

approximately the same as what is expected for a random distribution (the Mackenzie curve) [25]. Such a uniform microstructure meets the requirement of the present work.

Fig. 2 illustrates the GBPDs of ∑5 boundaries as filtered with angular deviations ±2.5° (Fig. 2a) and ±6.7° (Brandon criterion, Eq. (1)) (Fig. 2b). We can see that a maximum with a value of 1.54 MRD appears at the position of (0 1 3) (Fig. 2a). Taking (h_1 k_1 l_1) as (0 1 3), Eq. (2) yields (h_2 k_2 l_2) equal to (0 −1 3). Because (0 −1 3) is also a maximum in the distribution (Fig. 2a), it is believed that a specific GBIC of (0 1 3)/(0 −1 3) is favored for the ∑5 boundaries. Other maxima in the distribution found at (3 0 1), (3 1 0), (3 −1 0) and so on (the white arrows pointed at in Fig. 2a) are related by symmetry to those found at (0 1 3) and (0 −1 3). Therefore, the general GBIC is {0 1 3}/{0 1 3}. Because no other maxima are observed, it is believed that the GBIC of {0 1 3}/{0 1 3} is the primary component of the ∑5 boundaries with smaller angular deviations (±2.5°). As to the ∑5 boundaries with larger angular deviations (±6.7°), we can see that, in addition to {0 1 3}/{0 1 3}, two additional weaker GBICs of {0 0 1}/{0 0 1} (the black arrows pointed

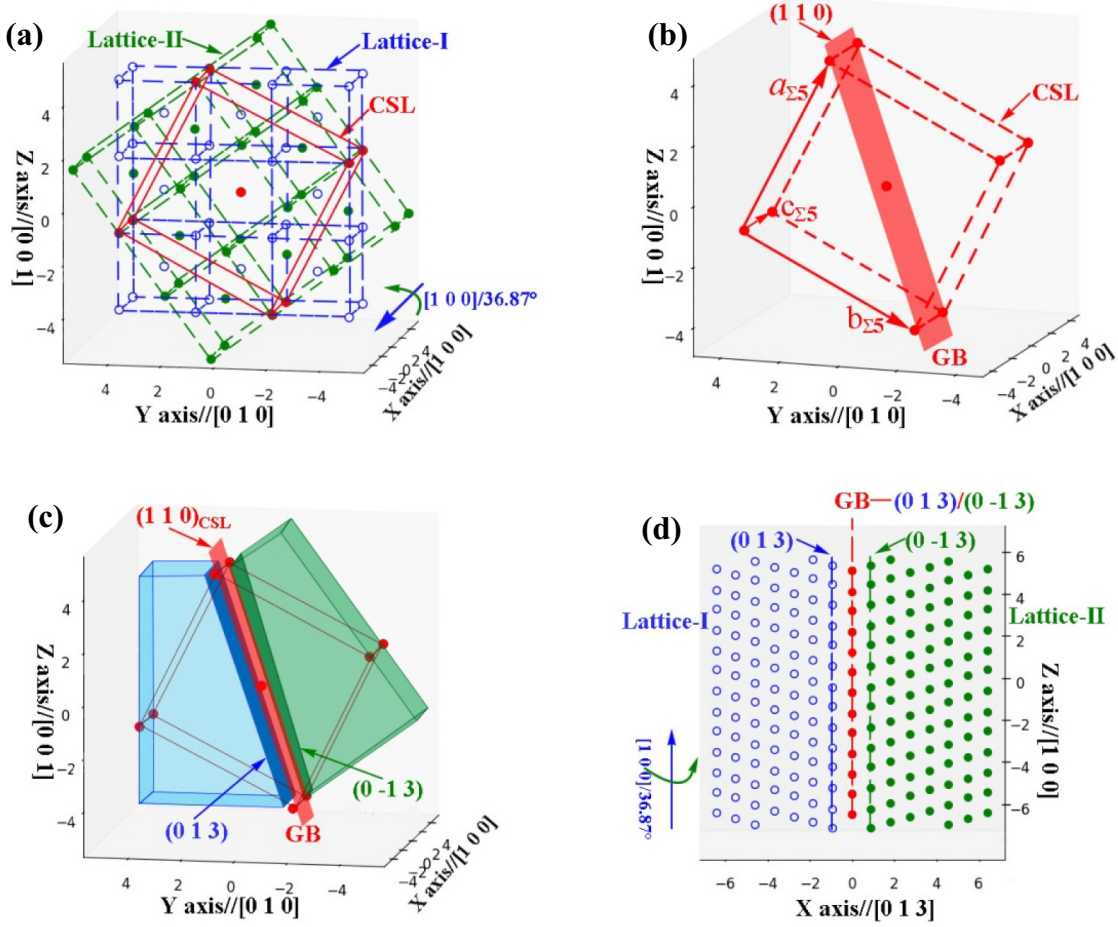

Fig. 3. Schematic illustrations of the structure of the ∑5 boundary with the (0 1 3)/(0 −1 3) GBIC. (a) Lattice misorientation and the ∑5 CSL super lattice. (b) The unit cell of the ∑5 CSL super lattice. (c) GB location showing the coincidence of $(1\ 1\ 0)_{CSL}$ with (0 1 3) and (0 −1 3) of the matrix. (d) (0 1 3)/(0 −1 3) symmetrical tilt boundary viewed on (0 −3 1).

at in Fig. 2b) and {3 2 5}/{3 2 5} (the white arrows pointed at in Fig. 2b) are also found. Obviously, the {0 1 3}/{0 1 3} GBIC should be attributed to the ∑5 boundaries with angular deviations less than ±2.5° as discussed above, and the other two must be related to those with angular deviations ranging from ±2.5° to ±6.7°.

The results in Fig. 2 suggest that the GBICs of ∑5 boundaries in iron are selective rather than random. {0 1 3}/{0 1 3} is the primary component among the GBICs of ∑5 boundaries. Because the sample was of high purity and had a uniform microstructure, the effects of impurities and texture should be negligible. Therefore, the observed GBICs of ∑5 boundaries are thought to be a reflection of the intrinsic behavior of iron. A possible origin for the preference for this GBIC is discussed below.

Fig. 3 shows a schematic illustration of the lattice misorientation and GB location of a ∑5 boundary with a (0 1 3)/(0 −1 3) GBIC. We can see in Fig. 3a, that the two adjacent grains (Lattice-I and Lattice-II) have a misorientation of [1 0 0]/36.87°. This results in a coincidence site lattice (CSL) [17] with ∑ = 5. The CSL is a super lattice with a body centered tetragonal unit cell that has lattice parameters of $a_{\sum 5} = b_{\sum 5} = \sqrt{5}a$ and $c_{\sum 5} = a$ (Fig. 3b). In this case, $a = 0.28664$ nm, which is the lattice parameter of BCC iron. It is easy to see the $(1\ 1\ 0)_{CSL}$ is the closest packed plane (CPP) of the CSL super lattice and it is coincident with (0 1 3) and (0 −1 3) of the matrix. This means that a ∑5 boundary with a (0 1 3)/(0 −1 3) GBIC locates its GB plane exactly on the CPP of the CSL super lattice (Fig. 3c) by which a symmetrical tilt boundary is formed (Fig. 3d). The preference for this GBIC might be related to its planar coincident site density (PCSD) [1]. Among the observed GBICs, the (0 1 3)/(0 1 3) GBIC has the maximum PCSD for ∑5 boundaries (the PCSDs of (0 1 3)/(0 −1 3), (0 0 1)/(0 0 1) and (3 2 5)/(3 −2 5) are 7.34/nm^2, 0.86/nm^2 and 0.14/nm^2, respectively). PCSD is a geometrical factor that might influence the GB energy and this might be the dominant factor influencing the formation of the GBIC of (0 1 3)/(0 −1 3) in present work. The reason is that the higher the PCSD, the higher the atomic ordering per unit area is in the GB region according to CSL theory [17]. Higher atomic ordering per unit area means a lower density of defects (such as free volume and dislocations) and a lower GB energy. However, this assumes the PCSD is the dominant factor that determines the GB energy. The present work shows the (0 1 3)/(0 −1 3) GBIC is the most common among all ∑5 boundaries, suggesting that it is preferentially selected during microstructure evolution. This analysis agrees well with the previous experimental results [26] showing that GBs of larger population usually have lower GB energy.

Fig. 4a shows an individual ∑5 boundary with a {0 1 3}/{0 1 3} GBIC identified by Wright's method [27] Fig. 4b and c illustrate the atomic configurations of the {0 0 1}/{0 0 1} and {3 2 5}/{3 2 5} GBICs of the ∑5 boundaries with angular deviations of 3° and 6.7°, respectively. It can be seen the atomic configurations in the two GBICs are quite different from that in the random GBs. The periodic groups of near coincident sites (NCS) or the so-called good matching sites (GMSs) [28,29] enclosed by the dotted lines reveal partial atomic ordering. As the authors discussed usin partial atomic ordering. As the authors discussed using O-lattice theory [30,31] in their previous work [2], such GBs

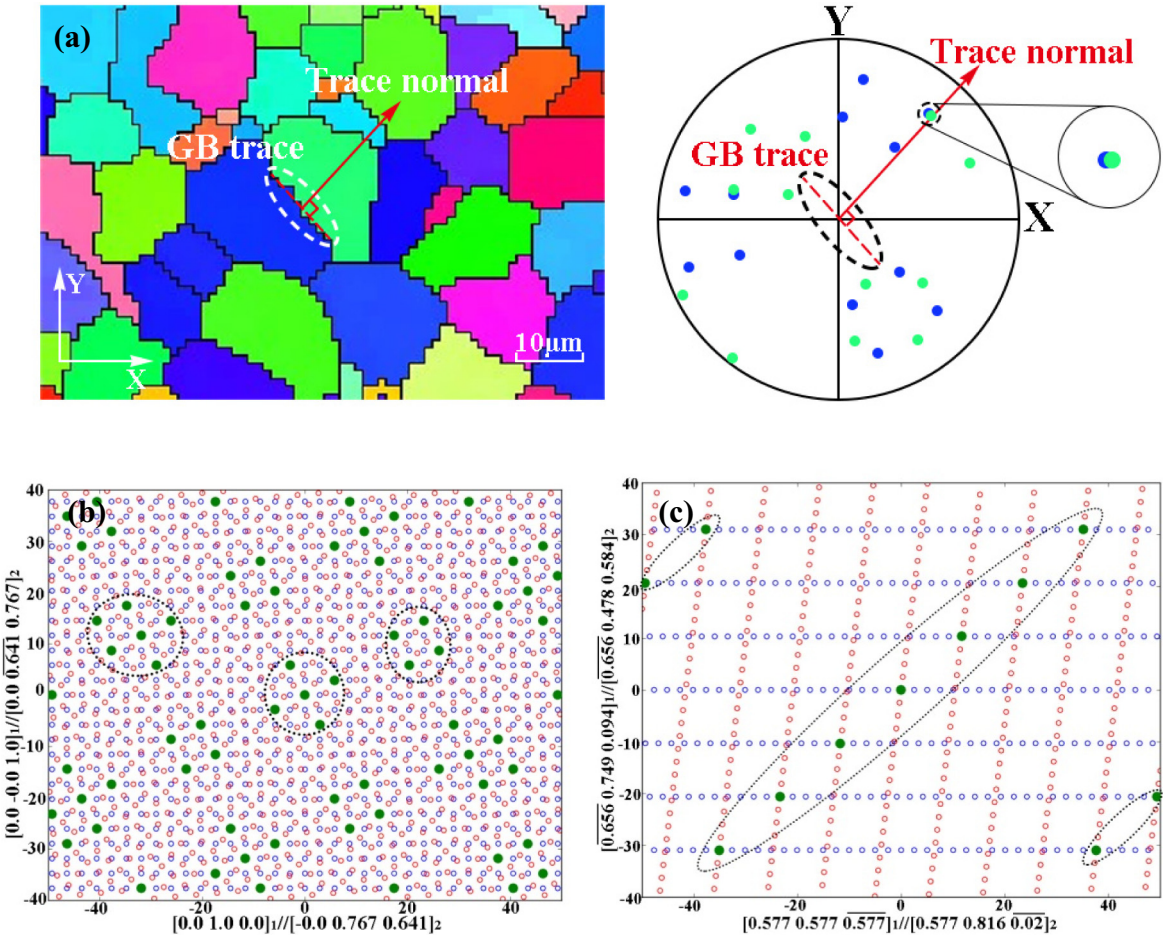

Fig. 4. A individual ∑5 boundary with a {0 1 3}/{0 1 3} GBIC identified by Wright's method in which the criterion is that the GB trace normal in the OIM is passing through the coincident {0 1 3} poles in the overlapped {0 1 3} pole figures of the two adjacent grains (a), and schematic illustrations of atomic configurations of {0 0 1}/{0 0 1} (b) and {3 2 5}/{3 2 5} (c) GBICs of ∑5 boundaries with angular deviations of 3° and 6.7°, respectively. The blue and red circles in (b) and (c) denote lattices of the abutted two grains, while the green dots are the NCS with a criterion of 0.1576 *a*. (*a* is the lattice parameter of BCC iron). (For interpretation of the references to color in this figure legend, the reader is referred to the web version of this article.)

usually have regular dislocation structures with lower energy compared to the random GBs, so they are formed preferentially during microstructure evolution.

In summary, the GBICs of ∑5 boundaries in a high purity iron with uniform microstructure are not random, showing a preference for {0 1 3}/{0 1 3}. This GBIC has the maximum PCSD and might possess the lowest GB energy if the geometrical factors are the most important. Meanwhile, {0 0 1}/{0 0 1} and {3 2 5}/{3 2 5} GBICs are also present and such ∑5 boundaries are different from the random boundary because of the periodic GMSs. Because impurities and orientation texture are not expected to influence this experiment, the current results should reflect the intrinsic behavior of the material and thus, are of general significance for BCC metals. If it is possible to grain boundary engineer BCC metals with ∑5 boundaries, then the concentration of the {0 1 3}/{0 1 3} GBIC should be maximized, just like we maximize ∑3 boundaries with the {1 1 1}/{1 1 1} GBIC in the grain boundary engineering of low to medium SFE FCC metals [32,33]. Of course, it should be noted that the frequency of ∑5 boundaries in the present work is fairly low. This is attributed to the uniform microstructure in which the grain boundary distribution is relatively isotropic. The introduction of some specific textures into the material could be a promising approach to obtain a higher frequency of ∑5 boundaries. For example, a ⟨0 0 1⟩∥ND fiber texture (ND means the normal direction of a plate rolled) would increase the frequency of ∑5 boundaries because this texture would limit the boundaries to misorientations around ⟨0 0 1⟩. Once again, it is emphasized that to pursue a high frequency of ∑5 boundaries is only one side of the issue, to pursue a high frequency of ∑5 boundaries with the {0 1 3}/{0 1 3} GBIC is the key point.

Acknowledgements

This work was supported by National Natural Science Foundation of China under the contract Nos. 51171095 and 51271058. The authors are grateful to Professor Wenzheng Zhang from Tsinghua University for her suggestions and discussions concerning the issue of near coincident site of grain boundaries.

References

[1] W.G. Wang, S. Chen, G.S. Rohrer, W.Z. Chen, Scr. Mater. 128 (2017) 18–22.
[2] W.G. Wang, C.H. Cai, G.S. Rohrer, X.F. Gu, Y. Lin, S. Chen, P.Q. Dai, Mater. Charact. 144 (2018) 411–423.
[3] P.H. Pumphrey, Scr. Metall. 6 (1972) 107–114.
[4] V. Randle, B. Ralph, J. Mater. Sci. 23 (1988) 934–940.
[5] G. Palumbo, K.T. Aust, Scr. Metall. 24 (1990) 1771–1776.
[6] E. Tochigi, Y. Kezuka, N. Shibata, A. Nakamura, Y. Ikuhara, Acta Mater. 60 (2012) 1293–1299.
[7] Y. Buranova, H. Rosner, S.V. Divinski, R. Imlau, G. Wilde, Acta Mater. 106 (2016) 367–373.
[8] A.D. Banadaki, S. Patala, Comput. Mater. Sci. 112 (2016) 147–160.
[9] D. Wolf, S. Yip, Materials Interfaces, Atomic-level Structure and Properties, Chapman & Hall, London, 1992.
[10] T. Watanabe, Res. Mech. 11 (1984) 47–52.
[11] G. Palumbo, K.T. Aust, Phys. Status Solidi A 131 (1992) 425–428.
[12] W.G. Wang, Y. Dai, J.H. Li, B.X. Liu, Cryst. Growth Des. 11 (2011) 2928–2934.
[13] G. Palumbo, U. Erb, MRS Bull. 11 (1999) 27–32.
[14] W.G. Wang, F.X. Yin, H. Guo, H. Li, B.X. Zhou, Mater. Sci. Eng. A491 (2008) 199–206.
[15] W.G. Wang, B.X. Zhou, G.S. Rohrer, H. Guo, Z.X. Cai, Mater. Sci. Eng. A527 (2010) 3695–3706.
[16] P. Lin, G. Palumbo, U. Erb, K.T. Aust, Scr. Metall. Mater. 33 (1995) 1387–1392.
[17] M.L. Kronber, Trans. AIME 185 (1949) 501–514.
[18] K.T. Aust, J.W. Rutter, Trans. AIME 215 (1959) 119–125.
[19] M. Pellan, S. Lay, J.M. Missiaen, Acta Mater. 167 (2019) 197–209.
[20] G.S. Rohrer, D.M. Saylor, B.E. Dasher, B.L. Adams, A.D. Rollett, P. Wynblatt, Z. Metall. 95 (2004) 197–214.
[21] D.M. Saylor, B.E. Dasher, B.L. Adams, G.S. Rohrer, Metall. Mater. Trans. A35 (2004) 1981–1989.
[22] D.G. Brandon, Acta Metall. 14 (1966) 1479–1484.
[23] V. Randle, Scr. Mater. 54 (2006) 1011–1015.
[24] X.Y. Huang, The Microstructure of Materials and Its Electron Microscopy Analysis, Metallurgical Industry Press, Beijing, 2008.
[25] J.K. Mackenzie, Biometrika 45 (1958) 229–240.
[26] G.S. Rohrer, J. Li, S. Lee, A.D. Rollett, M. Groeber, M.D. Uchic, Mater. Sci. Technol. 26 (2010) 661–669.
[27] S.I. Wright, R.J. Larsen, J. Microsc. 205 (2002) 245–252.
[28] W.Z. Zhang, G.C. Weatherly, Mater. Sci. 50 (2005) 181–292.
[29] W.Z. Zhang, Appl. Phys. Lett. 86 (2005) 1219–1222.
[30] W. Bollmann, Crystal Defects and Crystalline Interfaces, Springer, Berlin, 1970.
[31] W. Bollmann, Phys. Status Solidi (1974) 543–550 A21.
[32] V. Randle, Acta Mater. 47 (1999) 4187–4196.
[33] W.H. Yin, W.G. Wang, X.Y. Fang, Sci. Sin. Tech. 47 (2017) 1189–1197.